

# Numerical investigation of porous materials for trailing edge noise reduction

*International Journal of Aeroacoustics*

2020, Vol. 19(6–8) 347–364

© The Author(s) 2020

Article reuse guidelines:

[sagepub.com/journals-permissions](http://sagepub.com/journals-permissions)

DOI: 10.1177/1475472X20954410

[journals.sagepub.com/home/jae](http://journals.sagepub.com/home/jae)

Lennart Rossian , Roland Ewert and Jan W Delfs

## Abstract

In the framework of the German Collaborative Research Center *CRC 880: Fundamentals of High Lift for Future Civil Aircraft* porous materials as a means towards the reduction of airfoil trailing edge noise are investigated. At DLR, both experimental and numerical approaches are pursued to understand the physics behind the noise reduction. The present paper focuses on the numerical investigations, for which the experimental data serves as an evaluation basis. From the analysis of homogeneous materials, first steps are made towards the design of aeroacoustically tailored materials. It is assumed that materials with locally varying permeability may be suitable to achieve maximum noise reduction, as they provide a smooth transition from the solid airfoil to the free flow in the wake. The simulation results support this understanding, however it is revealed that high local gradients in the material properties themselves may act as acoustic sources.

## Keywords

Trailing edge noise, porous materials, computational aeroacoustics, tailored materials, validation

Date received: 31 January 2020; accepted: 2 August 2020

## Introduction

Due to the past and projected increase in commercial air traffic,<sup>1</sup> the noise emission from transport aircraft has become an important topic in research and politics.<sup>2,3</sup> Furthermore,

---

German Aerospace Center (DLR), Institute of Aerodynamics and Flow Technology, Braunschweig, Germany

### Corresponding author:

Lennart Rossian, German Aerospace Center (DLR), Institute of Aerodynamics and Flow Technology, Lilienthalplatz 7, Braunschweig 38108, Germany.

Email: [lennart.rossian@dlr.de](mailto:lennart.rossian@dlr.de)

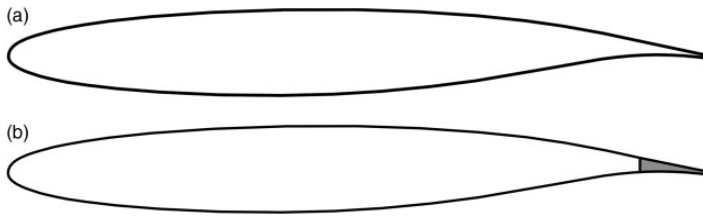


**Figure 1.** Airfoil DLR F16 as used for the experimental and numerical investigations with modification of the rear 10% of the chord length. (a) solid trailing edge. (b) porous trailing edge.

the demands for renewable energy has led to increased installation numbers of wind turbines, for which noise plays a major role for the certification. In both fields, the broadband turbulent boundary layer trailing edge noise (TBL-TEN) is one significant contributor.<sup>4</sup> This trailing edge noise is generated by the interaction of turbulent eddies with the pointed edge of the airfoil, representing a geometric discontinuity.<sup>5</sup>

There exists a variety of active and passive measures for the reduction of airfoil trailing edge noise. On the one hand, active methods are usually based on local blowing or boundary layer suction.<sup>6–10</sup> On the other hand, passive devices without energy supply are also promising. These often aim to alter the boundary layer turbulence, for example with boundary layer fences or rails.<sup>11–13</sup> Other approaches use rigid, porous materials.<sup>14–19</sup> Here, the noise reduction is based on a ventilation through the porous trailing edge, allowing for a turbulence pressure compensation between the upper and the lower side of the airfoil. Thereby, the discontinuity of the trailing edge is smoothed.<sup>20–22</sup> Further investigations consider similar porous materials to change the flow and noise radiation at blunt trailing edges.<sup>23,24</sup>

The airfoil used in the present contribution is the DLR F16, as sketched in Figure 1 with solid and porous trailing edge. The investigations are carried out at wind tunnel model scale, with an airfoil chord length of 300 mm, a free stream velocity of  $U_\infty = 50$  m/s and an angle of attack of  $\alpha = 0^\circ$ . The porous section extends over the rear 10% of the chord.

For the porous trailing edges, different aluminum materials are used. Figure 2 shows CT scans of three different materials, differing significantly in their structure. All these materials are rigid, though permeable due to their open pore structure. The first two materials show the range of pore sizes that were realized. The numbers in the naming are chosen accordingly (PA80-110 and PA200-250). The chosen materials cover a great range of pore sizes. The upper limit to the pore size is determined by the structural stability of the trailing edge, while for very small pores the permeability can get too small so that acoustic effects might not be observable. Using aluminum as a base material offers the possibility for easy machining. As an example, the last material is a modified version of the second (PA200-250). It was run through a cold rolling process to modify its inner structure. The scan reveals, that the material is more dense on the left side, where it is attached to the solid part of the airfoil. This is achieved by a variable infeed during the rolling.

## Numerical method

To simulate the influence of porous materials on airfoil trailing edge noise, a two-step hybrid CFD/CAA procedure is applied, that separates the computation of a steady flow field from the unsteady acoustic simulation. This approach was already successfully applied for trailing

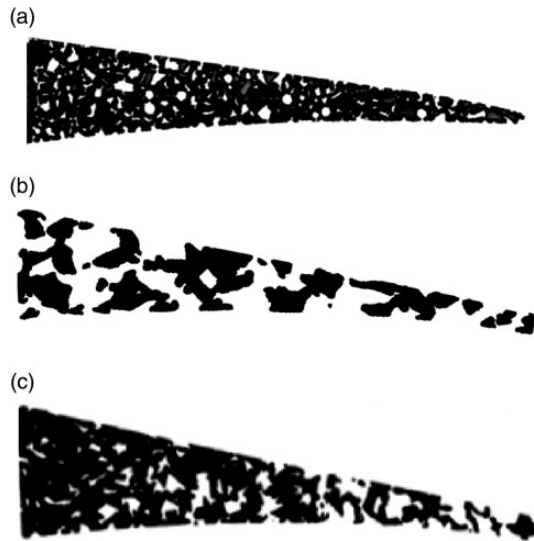


**Figure 2.** CT scans of exemplary porous trailing edges with different pore sizes and additional cold rolling process with varying infeed as provided by the Institute for Materials at TU Braunschweig.<sup>25</sup> (a) PA80-110. (b) PA200-250. (c) PA200-250, cold rolled.

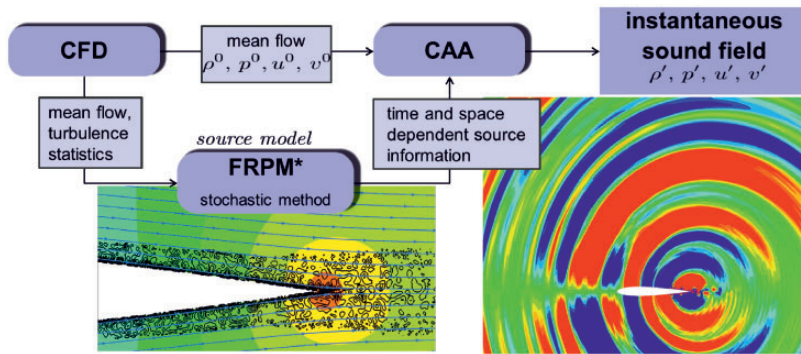


**Figure 3.** Flow chart to illustrate the two-step hybrid CFD/CAA approach.<sup>32</sup>

edge noise simulations.<sup>26</sup> Figure 3 shows a flow chart that presents the different stages. In the first step, DLR’s RANS flow simulation code TAU is used, that provides the ability to model porous materials by a volume-averaging approach<sup>27</sup> that will be presented in the following. Also the influence of the porous material on the turbulence is modeled by an extended Reynolds stress turbulence model.<sup>28</sup> From the flow simulation, information about the steady flow and the turbulence statistics is used to generate the unsteady turbulent sources by the stochastic turbulence reconstruction method fRPM (fast Random Particle Mesh method).<sup>29</sup> Therein, a white noise field is filtered to represent the velocity fluctuations of the turbulent structures based on the turbulence kinetic energy and the turbulence length

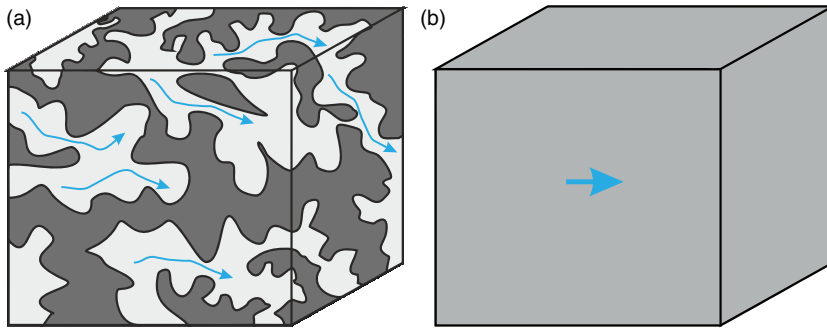


**Figure 4.** Sketch to illustrate the numerical modeling of porous materials. (a) microscopic structure. (b) volume-averaged representation.

scale from the turbulence model in the RANS simulation. The unsteady sources are then coupled into DLR's finite-differences CAA code PIANO<sup>30</sup> to calculate the acoustic propagation by solving the Acoustic Perturbation Equations (APE).<sup>31</sup>

To model porous materials in CFD and CAA simulations, two common approaches are possible. On the one side, a discretization of the microscopic structures can be implemented<sup>33</sup> to resolve the flow details (Figure 4(a)). Therefore, material scans can be used to obtain the necessary information about the inner structure.<sup>25,34</sup> In this approach, no approximation of the flow inside the pores is needed. However, due to the small pore sizes of about 1 mm and less, the numerical effort becomes too high to consider a vast variety of materials. Hence, this approach is not suitable for design studies. On the other side, porous materials can be modeled by characteristic parameters that give a volume-averaged formulation of the governing equations (Figure 4(b)). The parameters used in this contribution are the porosity  $\phi$ , permeability  $\kappa$  and the Forchheimer coefficient  $c_F$ . The porosity is a geometric parameter, giving the fluid volume inside a given total volume of porous material. Permeability and Forchheimer coefficient on the other hand yield information about the drag affecting flow through the material. Figure 5 shows the volume-averaged representation of the materials illustrated in Figure 2. It can be seen how the coarse material yields the highest permeability and how the deformation of the pores due to the cold rolling process results in a locally varying permeability. For small local flow velocity, the drag inside the material is dominated by viscous effects and can be described by the Darcy law (equation (1))<sup>35</sup> with  $p$  as static pressure,  $[u_i]$  as the local flow velocity vector and  $\mu$  as the fluid viscosity. The porous material is modeled by its porosity  $\phi$  and permeability  $\kappa$ . With increasing flow speed turbulent drag becomes relevant, which is accounted for by extending the Darcy law with a term formulated by Forchheimer (equation (2))<sup>36</sup> that takes the Forchheimer constant  $c_F$  as an additional parameter. With these material parameters, a volume-averaged formulation of the Linearized Euler Equations (LEE) in perturbation form can be found (equations (3) to (5)),<sup>32,37</sup> with  $\rho$  as the fluid density,  $\gamma$  the isentropic expansion factor,  $e_i$  the unity vectors of the coordinate system and  $\delta_{ij}$  the Kronecker delta. In the present perturbation form,  $\rho^0$ ,  $[u_i]^0$ ,  $p^0$  denote quantities of the constant mean flow field, while  $\rho'$ ,  $[u_i]'$ ,  $p'$  denote the perturbation variables.

$$\frac{\partial p}{\partial x_i} = -\phi \frac{\mu}{\kappa} [u_i] \quad (1)$$

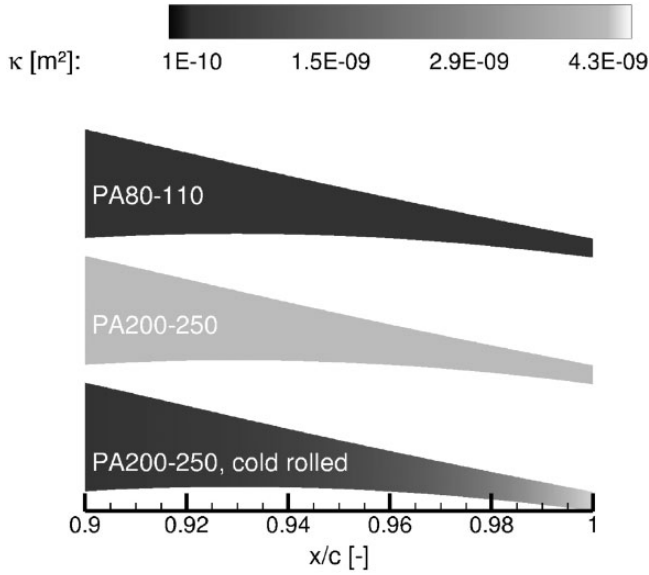


**Figure 5.** Examples for porous materials used to reduce trailing edge noise, with high, low and graded permeability.

$$\frac{\partial p}{\partial x_i} = -\phi \frac{\mu}{\kappa} [u_i] - \phi^2 \frac{c_F}{\sqrt{\kappa}} \rho [u_i]^2 \tag{2}$$

$$\frac{\partial \rho'}{\partial t} + [u_i^0] \frac{\partial \rho'}{\partial x_i} + [u_i'] \frac{\partial \rho^0}{\partial x_i} + \rho^0 \frac{\partial [u_i']}{\partial x_i} + \rho' \frac{\partial [u_i^0]}{\partial x_i} - \underbrace{\phi (\rho^0 [u_i'] + \rho' [u_i^0]) \frac{\partial}{\partial x_i} \frac{1}{\phi}}_{\text{gradient term}} = 0 \tag{3}$$

$$\begin{aligned} & \frac{\partial [u_i']}{\partial t} + [u_j^0] \frac{\partial [u_i']}{\partial x_j} + [u_j'] \frac{\partial [u_i^0]}{\partial x_j} + \frac{1}{\rho^0} \frac{\partial p'}{\partial x_i} - \frac{p'}{\rho^0 \rho^0} \frac{\partial p^0}{\partial x_i} + \dots \\ & + \underbrace{\phi \frac{\nu}{\kappa} \delta_{ij} [u_j']}_{\text{Darcy term}} + \underbrace{\phi^2 \frac{c_F}{\sqrt{\kappa}} \sqrt{[u_k^0][u_k^0]} [e_i^0 e_j^0 + \delta_{ij}]}_{\text{Forchheimer term}} [u_j'] - \underbrace{\phi \frac{p'}{\rho^0} \frac{\gamma - 1}{\gamma} \frac{\partial}{\partial x_i} \frac{1}{\phi}}_{\text{gradient term}} = 0 \end{aligned} \tag{4}$$

$$\frac{\partial p'}{\partial t} + [u_i^0] \frac{\partial p'}{\partial x_i} + [u_i'] \frac{\partial p^0}{\partial x_i} + \gamma \left( p^0 \frac{\partial [u_i']}{\partial x_i} + p' \frac{\partial [u_i^0]}{\partial x_i} \right) - \underbrace{\phi (p^0 [u_i'] + p' [u_i^0]) \frac{\partial}{\partial x_i} \frac{1}{\phi}}_{\text{gradient term}} = 0 \tag{5}$$

For the simulation of trailing edge noise with the presented CFD/CAA procedure, the Acoustic Perturbation Equations (APE) are solved.<sup>26,31</sup> These can be derived from the LEE by reformulating the momentum equation (4). Therefore the linearized Lambvector (with

$\epsilon_{ijk}$  representing the Levi-Civita symbol) is moved to the right hand side. Thus the turbulence reconstruction from fRPM can be directly imposed as a source term.

$$\begin{aligned} \frac{\partial [u_i']}{\partial t} + \frac{\partial [u_k^0][u_k']}{\partial x_j} + \frac{1}{\rho^0} \frac{\partial p'}{\partial x_i} - \frac{p'}{\rho^0 \rho^0} \frac{\partial p^0}{\partial x_i} + \underbrace{\phi \frac{\nu}{\kappa} \delta_{ij} [u_j']}_{\text{Darcy term}} + \underbrace{\phi^2 \frac{c_F}{\sqrt{\kappa}} \sqrt{[u_k^0][u_k^0]} [e_i^0 e_j^0 + \delta_{ij}] [u_j']}_{\text{Forchheimer term}} - \dots \\ - \underbrace{\phi \frac{p' \gamma - 1}{\rho^0 \gamma} \frac{\partial 1}{\partial x_i}}_{\text{gradient term}} = \underbrace{-\epsilon_{ijk} [\omega_j^0][u_k'] - \epsilon_{ijk} [\omega_j'] [u_k^0]}_{\text{linearized Lambvector}} \end{aligned} \quad (6)$$

With the presented approach to model porous materials by volume-averaging, special focus needs to be set to the formulation for the material interfaces to the free medium. In this work, a set of acoustic jump conditions is implemented to capture discontinuities of the primitive variables. Following a set of jump conditions used for RANS simulations,<sup>27,28</sup> conservation laws for mass flow, energy flow and entropy across the edges of porous sections are implemented (equations (7) to (9)).<sup>37</sup> As these jump conditions represent a general equilibrium state, they can be applied independently of the chosen governing equations (LEE or APE).

$$\rho' \phi [u_i^0] + \rho^0 \phi [u_i'] = \text{const} \quad (7)$$

$$\frac{\gamma}{\gamma - 1} \left( \frac{p'}{\rho^0} - \frac{p^0 \rho'}{(\rho^0)^2} \right) + [u_i^0][u_i'] = \text{const} \quad (8)$$

$$\frac{p'}{(\rho^0)^\gamma} - \gamma \frac{\rho' p^0}{(\rho^0)^2} = \text{const} \quad (9)$$

## Comparison with experimental results

In a first step, the simulation results for the solid and different porous trailing edges are compared to experimental data. This will give an insight to evaluate the quality of the numerical approach. To cover a wide range of different trailing edges, four different porous materials are used. These are listed in Table 1, with their respective porosity and permeability values. These parameters are determined at TU Braunschweig as a cooperation within the SFB 880.<sup>25</sup> While the porosity as a geometric quantity is calculated based on CT

**Table 1.** Material characteristics of different porous trailing edges used in simulations and measurements.

Name	Porosity $\phi$ (-)	Permeability $\kappa$ (m <sup>2</sup> )
PA80-110	0.46	$1.2 \cdot 10^{-10}$
PA120-150	0.55	$1.2 \cdot 10^{-9}$
PA200-250	0.57	$4.3 \cdot 10^{-9}$

scans of the material, the permeability is determined by measuring flow resistance through by an alternating flow at 1 Hz, as defined in the standard specification DIN EN 29053. The Forchheimer coefficient can not be determined by the experimental material characterization and is therefore neglected. A more detailed analysis shows that by neglecting the Forchheimer term the overall permeability of the porous material is slightly overestimated. However, it was found that the physical influence of the porous material on noise generation is still preserved.<sup>38</sup> While the porosity does not vary much between the materials, significant differences are notable in the permeability. This is related to different pore sizes, with the smallest pores in the PA80-110 and the largest in the PA200-250. All presented acoustic data is recorded for an angle of attack of  $0^\circ$  and a free stream velocity of 50 m/s. With the airfoil chord length of 0.3 m, this results in a Reynolds number of about  $1 \cdot 10^6$ . To ensure a fully developed turbulent boundary layer at the airfoil trailing edge, a zig-zag-tape is used for tripping. The tape is positioned at 5% of the airfoil chord on the suction side and at 10% on the pressure side. This setup was developed in previous flow measurements at TU Braunschweig to get a defined boundary layer state for different angles of attack.<sup>27</sup> Parallel to the flow measurements, 2D CFD computations of the airfoil in free flight condition were run. These simulations were run on a O-type mesh, with an average spacing of  $y^+ = 0.5$  at the viscous walls of the airfoil surface.<sup>27</sup> Inflow conditions and tripping were chosen as in the experiments, so that the setup could be directly used for the present aeroacoustic investigations.

To compare the simulation results to the experimental data, a virtual microphone is placed at  $90^\circ$  below the trailing edge at a distance of  $r_{sim.} = 1.5 \cdot c$  (with  $c$  being the airfoil chord length, giving  $r_{sim.} = 0.45$  m). As the simulations are run on a two dimensional mesh, the sound pressure levels have to be corrected to refer to the measurements which gives nominalized data for a wing span of  $b = 1$  m and a distance between trailing edge and microphone of  $r_{meas.} = 1$  m. The correction is needed, as the 2D simulations do not include the spanwise coherence length of the turbulent eddies at the trailing edge, which results in too high noise levels. The present approach is based on a model for the coherence length scales by Amiet<sup>39</sup> and is explained in detail by Ewert et al.<sup>40</sup> It follows equation (10) with the empirical constant  $C \approx 2.1$  and the free stream Mach number of  $Ma_\infty^0 = 0.15$  m/s at which the simulations and measurements are run. Additionally, a correction for the distance from trailing edge to microphone has to be applied, following the theoretical pressure decay in the far field (cf. equation (11)). To match the measurement spectra, a final shift of the corrected simulation spectra of -1.5 dB needs to be applied. This can be seen as a calibration and depends on the applied turbulence model in the flow computation.

$$SPL_{3D} = SPL_{2D} + 10 \log_{10} \left( \frac{C}{2\pi} \frac{b}{r_{sim.}} Ma_\infty^0 \right)$$

$$SPL_{3D} = SPL_{2D} - 9.5 \text{ dB} \quad (10)$$

$$p' \propto \frac{1}{r}$$

$$SPL_{meas.} = SPL_{sim.} + 20 \log_{10} \left( \frac{r_{sim.}}{r_{meas.}} \right)$$

$$SPL_{meas.} = SPL_{sim.} - 7 \text{ dB} \quad (11)$$

Figure 6 shows the direct comparison of the experimental and numerical data for the four different porous trailing edges to the solid reference. The spectra for the solid trailing edge show a very good agreement within an estimated  $\pm 1$  dB uncertainty range of the measurements<sup>41</sup> for frequencies above 2 kHz. In the low frequency domain the maximum of the simulated spectrum is found in the 1 kHz band, while the measured maximum is located in the 1.25 kHz band. This difference may be related to an increased uncertainty of the numerical data for low frequencies, due to a short sampling period of 0.1 s.

Comparing the data for the porous trailing edges, significant deviations between simulations and measurements are found. For the material PA80-110 with small pores and low permeability, the measurements show noise reduction of about 6 dB mostly in the high-frequency domain between 2 to 16 kHz (Figure 6(a)). The simulations predict a similar achievable noise reduction. However, here the reduction is found at lower frequencies between 1 to 4 kHz (Figure 6(a)). Simulation and measurement therefore both show that the influence of the porous trailing edge has a broadband character, but is limited to a specific frequency range. For the other, more permeable materials, even more distinct differences between experiment and simulation show up. In the measured spectra it can be seen that with rising pore size and permeability increasing high-frequency noise above 3 kHz comes up (Figure 6(b) and (c)). However, a around 1.25 kHz these materials show a

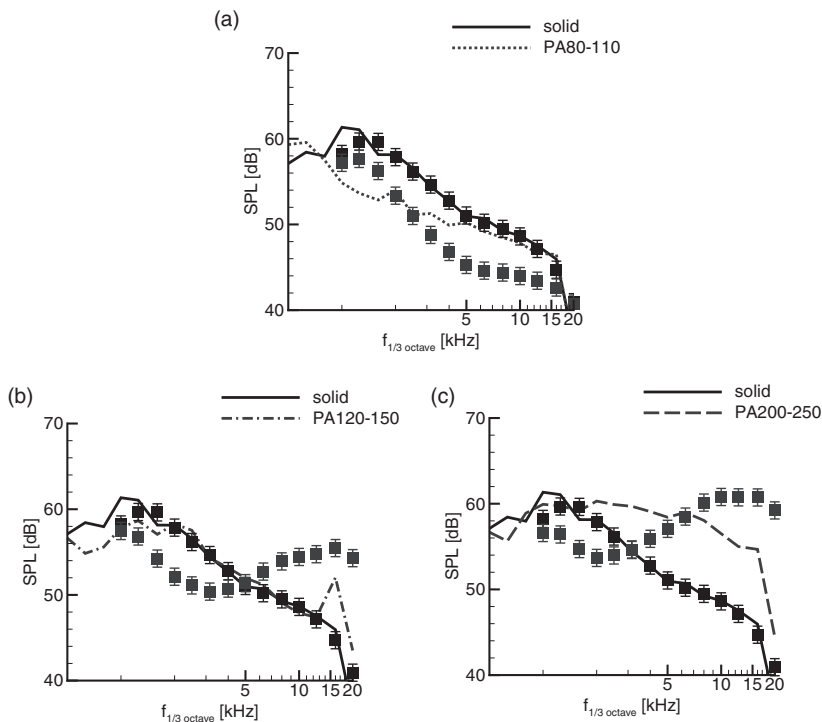


**Figure 6.** Comparison of 1/3-octave band spectra based on numerical (lines) and experimental (squares, with an estimated uncertainty of  $\pm 1$  dB<sup>41</sup>) for the solid and different porous trailing edges. The microphone position is located at 1 m below the trailing edge, free flow velocity is 50 m/s and the airfoil is installed at an angle of attack of  $0^\circ$ . (a) PA80-110: small pores, low permeability. (b) PA120-150: medium size pores, medium permeability. (c) PA200-250: large pores, high permeability.

higher noise reduction than the first, less permeable material PA80-110. The simulations of the materials with higher permeability however show only very limited noise reduction potential (Figure 6(b) and (c)). At this point it seems like the chosen numerical representation of the porous materials is not suitable to capture their effect on the reduction of trailing edge noise. Nevertheless, in some details the simulations give similar results as the experiments. One might consider that the high-frequency noise increase in the experiments is also present in the simulations, just with a more broadband character. In this case, the numerical approach might be useful to understand the noise reduction potential of porous materials applied to airfoil trailing edges. Therefore, the following sections will get into more detailed analysis of the simulation results.

## Analysis of noise generation

In the previous section it was shown that there are significant deviations between the numerical and experimental results, especially when it comes to highly permeable materials. In the following, a more detailed analysis is presented to provide a deeper understanding of the simulations. Therefore, the hybrid CFD/CAA approach is very useful. It enables to distinguish between the influence of the porous trailing edges on the conversion of turbulent to acoustic energy on the one side and on the turbulence itself on the other. In the first case, the source reconstruction of the solid airfoil is applied to the different porous trailing edges. In the second setup, the solid trailing edge is combined with turbulent sources based on the flow simulations of the porous edges. To give an impression on the influence of the porous trailing edges, Figure 7 illustrates the turbulence kinetic energy  $k^t$ , as calculated by the RANS flow simulation for the solid and the porous trailing edges. It can be clearly seen that the porous materials have a significant impact on the turbulence at the trailing edge. For each porous airfoil, an increase in the turbulence kinetic energy is present on the suction side. Simultaneously, due to flow penetration into the porous section, the turbulence intensity on the pressure side reduces with increasing permeability. This is driven by the pressure gradient between the bottom and top side of the cambered airfoil at  $\alpha = 0^\circ$ . Interestingly, the turbulence kinetic energy on the suction side is highest for the material PA80-110, which has the lowest permeability of the porous materials. It seems like for this case the local shear and therefore turbulence production in the flow is strongest. For the more permeable materials, the flow passing from the bottom side carries more momentum, which results in a more efficient mixing on the suction side and therefore less local turbulence. With respect to the previous results, the analysis of the turbulence gives a first hint that the observed noise increase for the more permeable materials might be related to the local flow at the trailing edge.

To get further into the analysis of the influence of porous materials, Figure 8(a) shows simulation results, when the turbulence information of the porous trailing edges are taken as source input for the stochastic turbulence reconstruction in fRPM with the solid airfoil in PIANO. This approach is possible, as the stochastic turbulence reconstruction in fRPM is separated from the acoustic computation in PIANO. It allows to distinguish between the influence of the porous trailing edge on the increase of turbulence, and hence the acoustic source on the one hand (Figure 8(a)) and the energy transfer from a specific turbulence source to acoustic energy on the other (Figure 8(b)). These two effects could never be separated in an experimental approach, as in reality both turbulence and energy transfer are determined by the porous trailing edge. Nevertheless, the artificial numerical approach gives valuable insights. It can be seen, that despite the significantly increased turbulence

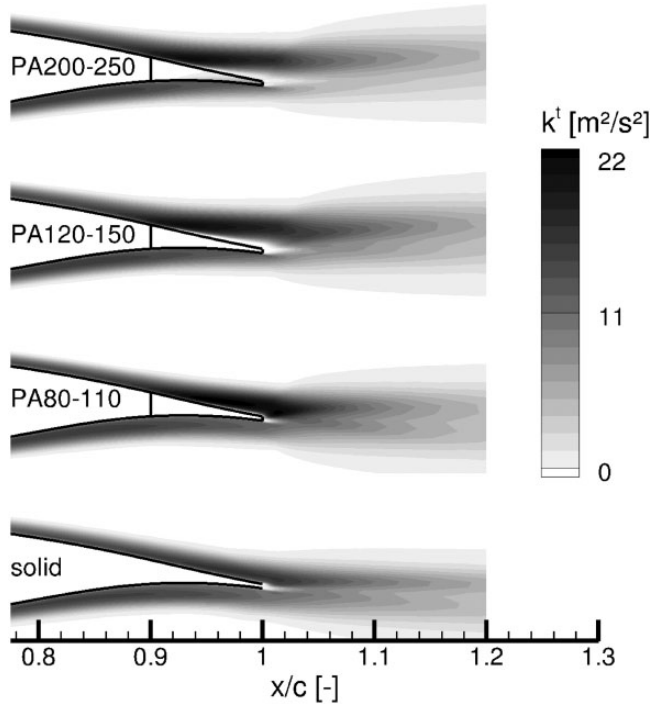


**Figure 7.** Contour plots of the turbulence kinetic energy  $k^t$  calculated by the RANS flow simulation for the solid and porous trailing edges.

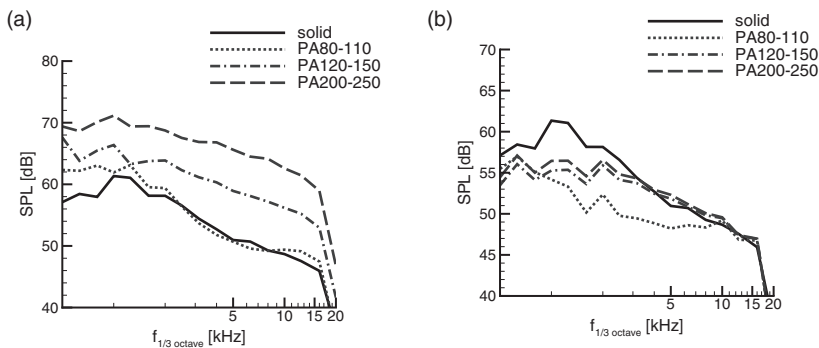


**Figure 8.** Simulation results for combination of different trailing edge materials with turbulence reconstruction based on flow computations of the solid or porous airfoil. (a) Solid trailing edge with turbulence from porous flow computation. (b) Porous trailing edges with turbulence from solid flow computation.

intensity observed for the PA80-110, over a wide frequency range the calculated spectrum agrees with the solid reference. The turbulence from the more permeable materials PA120-150 and PA200-250 however gives a strong broadband noise increase. The results suggest that the turbulence intensity at the trailing edge is not the most relevant measure for the

noise increase, but the local flow velocity on both suction and pressure side of the airfoil. However, the observed noise increase could be considered consistent with the measurements if it was limited to the high frequency domain. Thus, this shortcoming can partially explain the differences between simulation and experiment. All in all, the results give a hint that the high-frequency excess noise in the measurements might after all not only be due to roughness effects, but more to an alternated turbulence and mean flow field based on the flow passing through the porous section.

The influence of the porous materials on the turbulence at the airfoil trailing edge is only one part of the effect on the generation of trailing edge noise and does not explain the potential noise reduction. Therefore, Figure 8(b) shows simulation results when the turbulence reconstruction is based on the solid flow field and the acoustic computation is realized with different porous trailing edges. Here, all porous material give a broadband noise decrease. Interestingly, the material with lowest permeability provides the highest noise reduction, while the rising permeability from PA120-150 to PA200-250 only has very limited effect on the spectrum. To understand the reason, another simulation approach is pursued. Therein, not the entire turbulence field is reconstructed by superposition of synthetic eddies. Instead, a single vortex passing the trailing edge is simulated.

Figure 9(a) and (b) show snapshots of the acoustic pressure field at a constant simulation time. For the solid airfoil, the expected cardioid pattern with one wavefront and inversely phased radiation to the top and bottom is observed. In case of the porous trailing edge, made of PA80-110, the pressure field directly at the trailing edge shows a similar pattern, though with reduced sound pressure levels. The main difference between the two contour plots is found in the leading wave front that is present for the porous airfoil. It shows a similar cardioid, inversely phased pattern as the trailing edge signal. Here, the interaction of the vortex with the solid to porous intersection of the airfoil acts a discrete acoustic source location that is based on the same physical mechanism as the trailing edge noise. For a more detailed analysis of the influence of the different porous materials on the sound production at the intersection and the trailing edge, Figure 9(c) shows the time signal of a microphone at  $90^\circ$  below the trailing edge. As the sound radiation is symmetric to the upper and lower half plane of the airfoil, this analysis provides insight into the entire acoustic field. Similar to the presented snapshots the comparison of the signals from the solid and the porous trailing edge (PA80-110) shows a reduction of the trailing edge noise along with the new leading wave front originating from the solid-porous intersection. Moving on to the highly permeable materials PA120-150 and PA200-250, the intersection noise becomes the dominant source. This explains the limited overall noise reduction for increasing permeability as seen in Figure 8(b). The presented results are similar to a previous investigation with a NACA0012 airfoil.<sup>42</sup> Therein, a different source formulation was used in form of an analytical vortex that was transported by solving the Linearized Euler Equations. This similarity suggests that also for the present setup graded porous materials could be beneficial in terms of the achievable noise reduction. To evaluate the effect of such a material with locally varying permeability and porosity, the cold rolled version of the PA200-250 is applied<sup>25</sup> that provides a low permeability at the intersection and a high permeability at the trailing edge. The evaluated porosity and permeability from the experimental material characterization are shown in Figure 10. To get the material properties at the specific positions, multiple specimen of the base material are cold rolled to a constant thickness between 90% and 50% of the initial

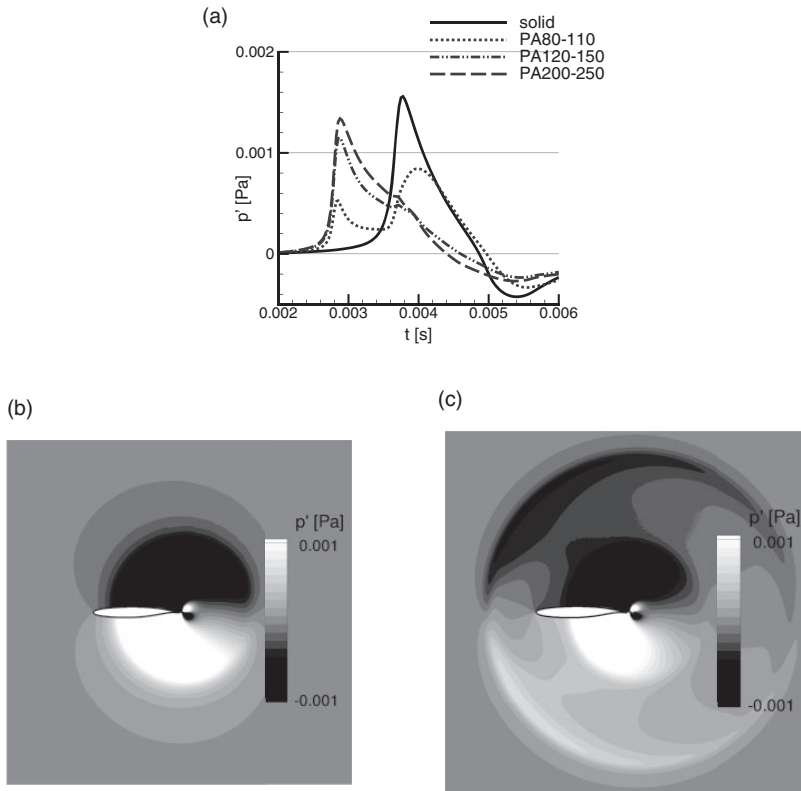


**Figure 9.** Simulation results for the realization of a single vortex as a representative acoustic source. (a) Contour plot of acoustic pressure for the solid airfoil at a simulation time of  $2.9 \cdot 10^{-3}$  s. (b) Contour plot of acoustic pressure for the porous airfoil with PA80-110 trailing edge at a simulation time of  $2.9 \cdot 10^{-3}$  s. (c) Time signal of the acoustic pressure registered by a microphone  $90^\circ$  below the trailing edge.

thickness. Then, each specimen is characterized by CT scan and flow measurement. As the inflection of the cold rolling for machining the trailing edge with locally varying properties is defined as a linear function in space, this approach determines an estimate of the local material characteristics. Figure 11(a) shows the time signal of the microphone from the simulation of the single vortex. It can be seen that the noise generated at the solid-porous intersection is reduced drastically, without making the trailing edge a distinct dominant source location. Instead, an acoustic wave is built over the entire time that the vortex passes above the porous section of the airfoil. By that, the conversion to acoustic energy is distributed, which helps to reduce the maximum pressure level. This reduction can also be observed in the simulation with turbulence reconstruction using the turbulence information from the flow of the solid airfoil (Figure 11(b), similar to Figure 8(b)).

## Design of aeroacoustically tailored materials

In good agreement with previous investigations, it was shown that porous materials with locally varying permeability are well suited to achieve a significant trailing edge noise

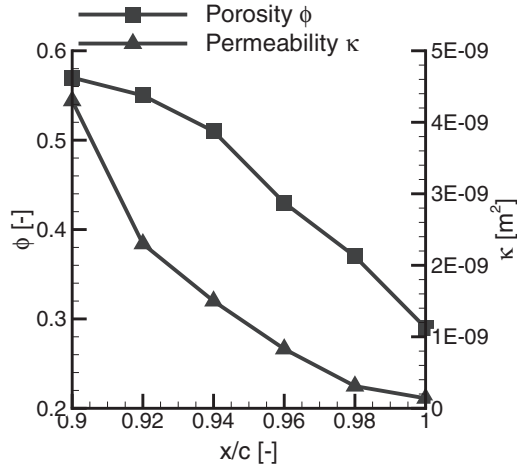


Figure 10. Porosity  $\phi$  and permeability  $\kappa$  used to model the cold rolled PA200-250 trailing edge.

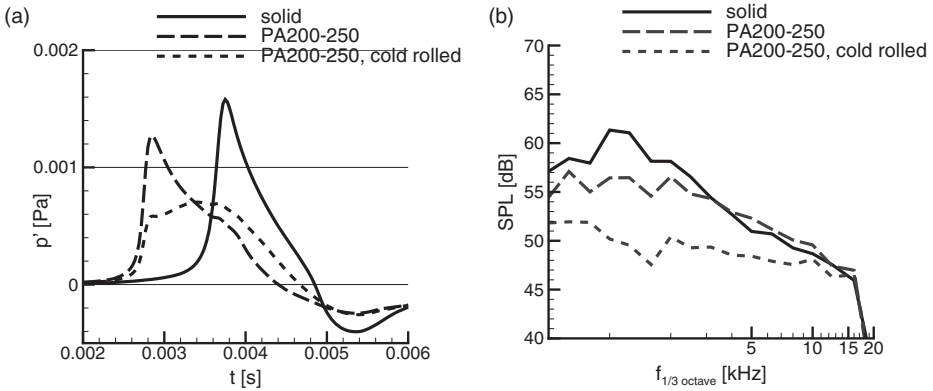
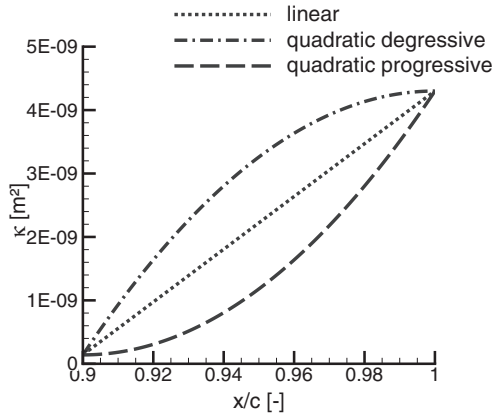


Figure 11. Simulation of a graded porous trailing edge from a cold rolled PA200-250. (a) Single vortex representation. (b) fRPM broadband simulation based on the turbulence statistics of the solid airfoil.

reduction. However, for design purposes it is desired to answer the question, which properties aeroacoustically tailored materials might have. To evaluate different graded materials, the least and the most permeable material of the preceding investigations (PA80-110 and PA200-250) are combined in different ways. Figure 12 shows three model functions to vary the permeability with fixed values at the solid-porous intersection at  $x/c = 0.9$  and the trailing edge at  $x/c = 1$ . First, a linear function is considered. Second, two quadratic functions are implemented. These are defined to have a zero gradient either at the intersection or the edge. This approach shall help to evaluate the effect of the gradient of the permeability. The porosity is kept constant at  $\phi = 0.5$ , as previous work has shown that variations in this value have only minor influence on the radiated noise.<sup>42</sup> The assumption that porosity can be kept constant for varying permeability is not necessarily valid for real porous materials.



**Figure 12.** Model functions for permeability to realize different graded porous materials with fixed values at start and end.

However, the characterization of the materials presented in Table 1 shows that for certain materials the permeability can in fact vary by one order of magnitude while the porosity only differs by about 20%.

Figure 13(a) reveals that the gradient of the permeability has a notable effect on the noise generation at the porous section of the airfoil. It can be seen that at the solid-porous intersection the acoustic signal increases with the gradient. For the zero gradient, the noise generation is about the same as for the homogeneous PA80-110 and is amplified by about 70% for the material with the highest local gradient. At the trailing edge, a similar trend is observed. However, the differences between the artificial materials are less prominent and the generated sound pressure levels are close to those of the homogeneous PA200-250. In previous investigations of a NACA0012 airfoil (shown in Figure 13(b)) a deviant trend was observed. Therein, the effect of the gradient was stronger at the trailing edge. It has to be noted that additionally to the changed airfoil geometry, also the permeability at the trailing edge of the porous section was lower ( $1 \cdot 10^{-9} \text{m}^2$  instead of  $4.3 \cdot 10^{-9} \text{m}^2$ ) and a different source realization was used. Thus, the time signals show a different form and the results are not directly comparable. However, the influence of the permeability gradient should be similar, as the modeling of the porous material is the same.

To examine whether the chosen start and end value of the permeability yields a major influence on the sound generation, further simulations with the F16 airfoil are run. Therein, the local permeability is halved compared to the model functions shown in Figure 12. To have a direct comparison, Figure 14(a) shows the same results as in Figures 13(a) and 14(b) those for the new materials with reduced permeability. In the new results, it shows that the influence of the gradient at the trailing edge is now stronger, despite its reduction of the factor of 2. For the sound generation at the intersection, an obverse trend is seen. Generally, the influence of the gradient is closer to the results obtained in the simulations with the NACA0012 airfoil. This concludes that the combination of the local gradient and the local value of the permeability is a crucial parameter to determine the generation of acoustic waves.

The preceding numerical results can also be backed by a theoretical analysis. From the porous volume-averaged formulation of the Linearized Euler Equations (equations (3) to (5)), a Poisson equation can be derived. Taking a constant porosity and the Forchheimer

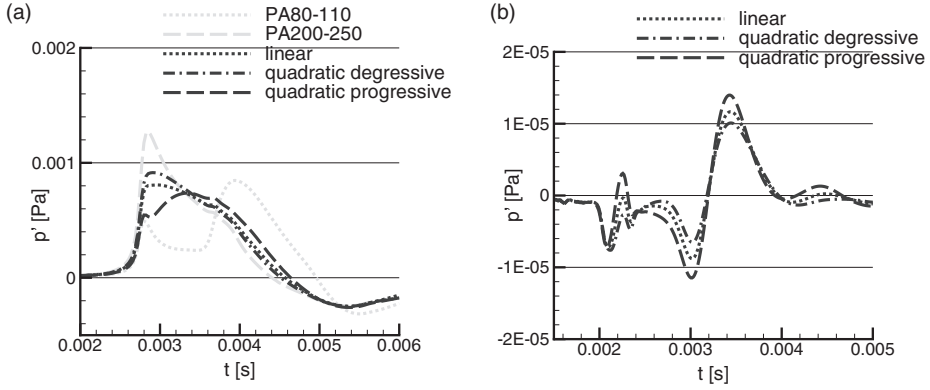


**Figure 13.** Microphone time signals of the trailing edge noise generated for graded porous materials applied to different airfoils. (a) F16 airfoil. (b) NACA0012 airfoil.<sup>42</sup>

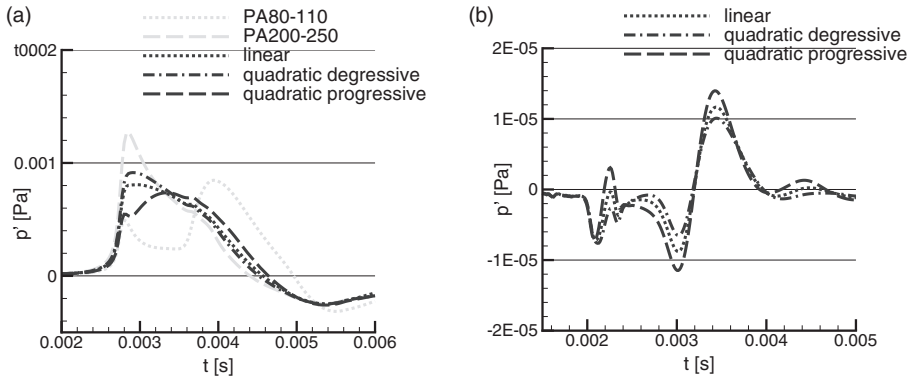


**Figure 14.** Microphone time signals of the trailing edge noise generated for graded materials on the F16 airfoil with different mean permeability. (a) Permeability as shown in Figure 12. (b) Permeability half the value as shown in Figure 12.

coefficient as zero, equation (12) is written. Note that in order to write the Poisson equation in non-dimensional form, the boundary layer thickness  $\delta$  and a mean permeability  $\bar{\kappa}$  based on the value at the solid-porous interface  $\kappa_1$  and the trailing edge  $\kappa_2$  are used. The second term on the right hand side includes the effect of the porous material. Note that it yields both the gradient as well as the local value of the permeability. Considering  $v'$  as the incident velocity field of a vortex passing a graded porous material, the inhomogeneous material acts as a source term for the local pressure. If this local pressure is furthermore diffracted at an edge (either the solid-porous intersection or trailing edge), it may be converted to an acoustic signal. This relates directly to the discussed simulation results.

$$\Delta p' = -\nabla \cdot \nabla \cdot (vv)' + \frac{Da}{Re} \frac{\phi}{\kappa^2} v' \cdot \nabla \kappa \tag{12}$$

$$Da := \delta^2 \bar{\kappa}, \quad Re := \frac{U_\infty \delta}{\nu}, \quad \bar{\kappa} = \frac{\kappa_1 + \kappa_2}{2}$$

## Conclusions

In the present paper it was shown that porous materials are suitable to reduce airfoil trailing edge noise. Despite significant deviations between the experimental and numerical results, the simulations show a consistent picture of the noise generation at a porous trailing edge. As in previous investigations, the solid-porous intersection of the airfoil was found to become the dominant noise source for highly permeable materials. From this finding it was concluded that graded porous materials, that yield a locally varying permeability might be a good choice to achieve maximum noise reduction. Simulations with differently tailored materials were carried out to support this idea. They revealed that graded materials have to be considered in the search for aeroacoustically optimized materials. However, strong local gradients of the permeability, especially at the solid intersection and the trailing edge may act as additional source locations.

Further effort will need to be put into the investigation of the deviations of the measurement and simulation results. Other simulation approaches, like Large Eddy simulations might help to understand if the chosen approach to model the turbulent sources is suitable to capture all effects of the porous materials on the turbulence. Furthermore, pore-resolving simulations could aid to verify the volume-averaging approach to model the materials.

## Acknowledgements

The experimental investigation of porous materials applied to an airfoil trailing edge were run by Karl-Stéphane Rossignol, Alexandre Suryadi and Michaela Herr from the Institute of Aerodynamics and Flow Technology at DLR.

Support to carry out the flow simulations was given by Pradeep Kumar from the Institute of Fluid Dynamics of TU Braunschweig in form of the computational mesh and advice on the input parameters for the TAU code.

Experimental characterization of the porous materials was done by Jörn Tychsen from the Institute for Materials and Christopher Blech from the Institute for Acoustics, both at TU Braunschweig.

## Declaration of conflicting interests

The author(s) declared no potential conflicts of interest with respect to the research, authorship, and/or publication of this article.

## Funding

The author(s) disclosed receipt of the following financial support for the research, authorship, and/or publication of this article: Financial support is provided by the German Research Foundation (Deutsche Forschungsgemeinschaft, DFG) in the framework of the Collaborative Research Center CRC 880. Computational resources are provided by German Aerospace Center (Deutsches Zentrum für Luft- und Raumfahrt e.V., DLR), Institute of Aerodynamics and Flow Technology.

## ORCID iD

Lennart Rossian  <https://orcid.org/0000-0002-2578-1195>

## References

1. Henke R, Lammering T and Anton E. Impact of an innovative quiet regional aircraft on the air transportation system. *J Aircr* 2010; 47: 875–886.

2. Dobrzynski W. Almost 40 years of airframe noise research: what did we achieve? *J Aircr* 2010; 47: 353–367.
3. European Commission. *Flightpath 2050: Europe's vision for aviation*. Belgium: European Commission, 2011.
4. Oerlemans S, Sijtsma P and Méndez López B. Location and quantification of noise sources on a wind turbine. *J Sound Vib* 2007; 299: 869–883.
5. Howe MS. Trailing edge noise at low Mach numbers. *J Sound Vib* 1999; 225: 211–238.
6. Gerhard T, Erbslöh S and Carolus T. Reduction of airfoil trailing edge noise by trailing edge blowing. *J Phys Conf Ser* 2014; 524: 012123.
7. Wolf A, Lutz T, Würz W, et al. Trailing edge noise reduction of wind turbine blades by active flow control. *Wind Energ* 2015; 18: 909–923.
8. Arnold B, Lutz T, Krämer E, et al. Wind-turbine trailing-edge noise reduction by means of boundary-layer suction. *AIAA J* 2018; 56: 1843–1854.
9. Szöke M, Fiscaletti D and Azarpeyvand M. Effect of inclined transverse jets on trailing-edge noise generation. *Phys Fluids* 2018; 30: 085110.
10. Szöke M, Fiscaletti D and Azarpeyvand M. Influence of boundary layer flow suction on trailing edge noise generation. *J Sound Vib* 2020; 475: 115276.
11. Clark I, Alexander WN, Devenport WJ, et al. Bioinspired trailing edge noise control. *AIAA J* 2017; 55: 740–754. <https://doi.org/10.2514/1.J055243>
12. Afshari A, Azarpeyvand M, Dehghan AA, et al. Trailing-edge flow manipulation using streamwise finlets. *J Fluid Mech* 2019; 870: 617–650.
13. Afshari A, Dehghan AA and Azarpeyvand M. Novel three-dimensional surface treatments for trailing-edge noise reduction. *AIAA J* 2019; 57: 4527–4535.
14. Hayden RE and Chanaud RC. Foil structures with reduced sound generation, US Patent 3853428, USA, 1974.
15. Herr M, Rossignol K-S, Delfs J, et al. Specification of porous materials for low-noise trailing-edge applications. In: *AIAA AVIATION forum, 20th AIAA/CEAS aeroacoustics conference*, Atlanta, GA, USA, 16–20 June 2014.
16. Geyer T, Sarradj E and Fritzsche C. Measurement of the noise generation at the trailing edge of porous airfoils. *Exp Fluids* 2010; 48: 291–308.
17. Schulze J and Sesterhenn J. Optimal distribution of porous media to reduce trailing edge noise. *Comput Fluids* 2013; 78: 41–53.
18. Bae Y and Moon YJ. Effect of passive porous surface on the trailing-edge noise. *Phys Fluids* 2011; 23: 126101.
19. Jiang C, Moreau D, Yauwenas Y, et al. Control of rotor trailing edge noise using porous additively manufactured blades. In: *2018 AIAA/CEAS aeroacoustic conference*, 2018.
20. Faßmann BW, Delfs JW, Ewert R, et al. Reduction of emitted sound by application of porous trailing edges. SFB 880 – fundamentals of high-lift for future commercial aircraft. Biennial Report, 2013.
21. Rubio Carpio A, Merino Martínez R, Avallone F, et al. Experimental characterization of the turbulent boundary layer over a porous trailing edge for noise abatement. *J Sound Vib* 2019; 443: 537–558.
22. Teruna C, Manegar F, Avallone F, et al. Noise reduction mechanisms of an open-cell metal-foam trailing edge. *J Fluid Mech* 2020; 898.
23. Ali SAS, Azarpeyvand M and da Silva CRI. Trailing-edge flow and noise control using porous treatments. *J Fluid Mech* 2018; 850: 83–119.
24. Koh S, Ryong Meinke M and Schroeder W. Numerical analysis of the impact of permeability on trailing-edge noise. *J Noise Vib* 2018; 421: 348–376.
25. Tyachsen J, Lippitz N and Rösler J. Modification of porous aluminum by cold rolling for low-noise trailing edge applications. *Metals* 2018; 8: 598.

26. Rautmann C, Dierke J, Ewert R, et al. Generic airfoil trailing-edge noise prediction using stochastic sound sources from synthetic turbulence. In: *AIAA AVIATION forum, 20th AIAA/CEAS aeroacoustics conference*, Atlanta, GA, USA, 16–20 June 2014.
27. Mößner M and Radespiel R. Flow simulations over porous media – comparisons with experiments. *Comput Fluids* 2017; 154: 358–370.
28. Mößner M and Radespiel R. Modeling of turbulent flow over porous media using a volume averaging approach and a Reynolds stress model. *Comput Fluids* 2015; 108: 25–42.
29. Ewert R. RPM – the fast random particle-mesh method to realize unsteady turbulent sound sources and velocity fields for CAA applications. In: *13th AIAA/CEAS aeroacoustics conference (28th AIAA aeroacoustics conference)*, Rome, Italy, 21–23 May 2007.
30. Delfs JW, Bauer M, Ewert R, et al. Numerical simulation of aerodynamic noise with DLR's aeroacoustic code PIANO, <https://elib.dlr.de/118928/> (2008, accessed 20 August 2020).
31. Ewert R and Schröder W. Acoustic perturbation equations based on flow decomposition via source filtering. *J Comput Phys* 2003; 188: 365–398.
32. Faßmann BW, Rautmann C, Ewert R, et al. Prediction of porous trailing edge noise reduction via acoustic perturbation equations and volume averaging. In: *AIAA AVIATION forum, 21st AIAA/CEAS aeroacoustics conference*, Dallas, TX, USA, 22–26 June 2015.
33. Kutscher K, Geier M and Krafczyk M. Multiscale simulation of turbulent flow interacting with porous media based on a massively parallel implementation of the cumulant lattice Boltzmann method. *Comput Fluids* 2019; 193: 103733.
34. Lippitz N, Blech C, Langer S, et al. Identification of material parameters for the simulation of acoustic absorption of fouled sintered fiber felts. *Materials* 2016; 9: 709.
35. Darcy H. 1856. Les fontaines publiques de la ville de Dijon, *Librarie des corps impériaux des ponts et chaussées et des mines*, <https://gallica.bnf.fr/ark:/12148/bpt6k624312.image> (accessed 20 August 2020).
36. Forchheimer P. Wasserbewegung durch boden. *Z Des Vereines Deutscher Ingenieure* 1901; 45: 50.
37. Rossian L, Ewert R and Delfs J. Evaluation of acoustic jump conditions at discontinuous porous interfaces. In: *AIAA AVIATION forum, 23rd AIAA/CEAS aeroacoustics conference*, Denver, CO, USA, 5–9 June 2017.
38. Rossian L. *Minderung der Schallabstrahlung von aktiven Hochauftriebssystemen mit porösen Materialien*. Doctoral Thesis, Technische Universität Braunschweig, Deutsches Institut für Luft- und Raumfahrt e.V., 2020.
39. Amiet R. Noise due to turbulent flow past a trailing edge. *J Sound Vib* 1976; 47: 387–393.
40. Ewert R, Appel C, Dierke J, et al. RANS/CAA based prediction of NACA 0012 broadband trailing edge noise and experimental validation. In: *15th AIAA/CEAS aeroacoustics conference (30th AIAA aeroacoustics conference)*, Miami, FL, USA, 11–13 May 2009.
41. Herr M. Trailing-edge noise- reduction concepts and scaling laws. Doctoral Thesis, Technische Universität Braunschweig, Deutsches Institut für Luft- und Raumfahrt e.V., 2013.
42. Rossian L, Ewert R and Delfs JW. Prediction of airfoil trailing edge noise reduction by application of complex porous material. In: Andreas D, Stephan B, Gerd H, Rolf R, Ewald K, Richard S, Claus W (eds) *New results in numerical and experimental fluid mechanics XI*, Germany: Springer International Publishing, 2018, pp. 647–657.